Decomposition in Ni-Co-Mn-In functional Heusler alloys and its effect on shell-ferromagnetic and magnetocaloric effects

M. Şaşmaz,[1] F. Dreist,[2] I. Iglesias,[2] A. Çakır,[3] M. Farle,[2,4] and M. Acet[2,*]

[1]*Department of Electricity and Energy, Gölbaşı Vocational School Adıyaman University, 02500 Adıyaman Turkey*

[2]*Faculty of Physics and CENIDE, Universität Duisburg-Essen, 47048 Duisburg, Germany*

[3]*Muğla University, Department of Metallurgical and Materials Engineering, 48000, Muğla, Turkey*

[4]*Kirensky Institute of Physics, Federal Research Center KSC SB RAS, Krasnoyarsk, 660036 Russia*

(Received 27 June 2020; revised 20 July 2020; accepted 21 July 2020; published 4 August 2020)

Ni-Co-Mn-In Heusler-based compounds are interesting for their magnetocaloric properties and have been widely investigated for this purpose. For Co compositions more than 5 at% in $(Ni_{100-x}Co_x)_{50}Mn_{25+y}In_{25-y}$ the material is no longer single phase, and for $y < 25$, shell-ferromagnetic precipitation occurs. Our study is twofold: First we study here the shell-ferromagnetic properties of these systems and show that their ferromagnetic exchange can be strengthened by introducing Co into the precipitate. Second, we further show that both the multiphase character and shell-ferromagnetic precipitation have strong implications on the magnetocaloric properties.

DOI: 10.1103/PhysRevB.102.064401

I. INTRODUCTION

The discovery of the martensitic transition in the Heusler compound $Ni_{50}Mn_{25}Ga_{25}$ set grounds to the later discovery of the magnetic shape memory effect in this compound [1,2]. A magnetic-field-induced strain in the martensite phase of up to 10% in $Ni_{50}Mn_{30}Ga_{20}$ [3] became the source of motivation for the search of this effect also in other Ni-Mn-Z martensitic Heusler materials (Z: Al, Ga, In, Sn, Sb) [4,5]. Although a magnetic-field-induced strain of this size was never found in any other compound, the research led to the discovery of even newer effects; these being the magnetic-field-induced reverse martensitic transitions [6,7], the inverse magnetocaloric effect [8], giant magnetoresistance [9,10], exchange bias [11,12], and shell-ferromagnetism [13]. The martensitic transformation in these materials is also exploited for energy conversion purposes [14].

Among all these functionalities, the magnetocaloric property, particularly in Ni-Mn-Sn- and Ni-Mn-In-based compounds, came to be recognized as being the most prominent [7,15–17]. Entropy changes around room temperature ranging up to 20 $Jkg^{-1}K^{-1}$ were reported in these materials and much work is still being carried out to improve the magnetocaloric properties; particularly those related to dealing with adverse transitional hysteresis effects [18–22].

A more recently observed feature of martensitic Heuslers is the shell-ferromagnetic (shell-FM) effect [13,23]. $Ni_{50}Mn_{50-x}Z_x$ alloys with $x \approx 5-10$ at% are antiferromagnetic (AF) and chemically homogeneous when annealed around 1100 K and then rapidly cooled to room temperature. When the alloy is subsequently annealed at around 600–750 K, it decomposes into FM $Ni_{50}Mn_{25}Z_{25}$ and AF $Ni_{50}Mn_{50}$ according to the reaction,

$$(25/x)Ni_{50}Mn_{50-x}Z_x \rightarrow Ni_{50}Mn_{25}Z_{25} + [(25/x)-1]Ni_{50}Mn_{50} \qquad 0 < x \leqslant 25. \tag{1}$$

For $x = 5$, a maximum of 20% of the decomposed sample can be made up of 2–5 nm cubic FM $Ni_{50}Mn_{25}Z_{25}$ precipitates when annealed at $T_a = 650$ K. The FM precipitates have a Curie temperature T_C of about 320 K and become embedded in a tetragonal AF $Ni_{50}Mn_{50}$ matrix. If this secondary heat treatment takes place under a magnetic field of several kilo Oersteds, then the magnetic moments at the FM/AF interface between the $Ni_{50}Mn_{50}$ matrix and the $Ni_{50}Mn_{25}Z_{25}$ precipitates pin along the field direction. When the temperature is reduced and afterwards the field removed, the spins remain pinned at temperatures $T_C < T < 550$ K. The coercive field of the pinning exceeds 20 T [24]. At $T > T_C$ the core of the precipitates is paramagnetic (PM), and the shell is FM with no T_C. The reason why it does not have a T_C is because the ferromagnetic ordering is not spontaneous as in a normal ferromagnet, but it is induced and aligned by the magnetic field applied on annealing and pinned by the AF exchange of the surrounding NiMn matrix. This effect has important relevance to permanent magnet and nonvolatile magnetic memory applications.

Decomposition effects in functional Heuslers by secondary heat treatment can have important implications on magnetocaloric effects. It turns out that all off-stoichiometric Ni-Mn-based Heuslers are chemically unstable, and there is a miscibility gap in $Ni_{50}Mn_{50-x}Z_x$ in the range of about $0 \leqslant x \leqslant 25$ according to Eq. (1). This raises questions on the influence of sample preparation procedures on magnetocaloric effects.

*mehmet.acet@uni-due.de

When Ni is partially replaced by Co in $Ni_{50}Mn_{50-x}Z_x$ compounds the martensitic transition decreases while T_C increases so that inverse and conventional magnetocaloric properties can be manipulated. A number of works have been carried out on the magnetocaloric properties of $(Ni_{1-y}Co_y)_{50}Mn_{50-x}Z_x$, and, indeed, an increase in the magnetocaloric effect and the broadening of the functioning temperature-range have been reported [22,25–27]. However, there are metallurgical homogeneity problems that remain to be solved. These are related to the shell-FM effect and to immiscibility issues [28–31].

There are two examples for this. The first is the case for Z taken as Ga. The end compositions in this series are stable so that single-phase samples with $0 \leqslant y \leqslant 1$ can be obtained. However, if $x < 25$, then the sample can decompose when it is subjected to secondary heat treatment as was shown for $y = 0$ [32]. The second example is for Z as In. $Co_{50}Mn_{50-x}In_x$ is not a stable compound so that the Co-composition in $(Ni_{1-y}Co_y)_{50}Mn_{50-x}In_x$ can only be limited. This is a purely miscibility limitation on top of which comes the shell-FM precipitation on applying secondary heat treatment. In this work, we study (i) shell-ferromagnetism in $(Ni_{1-y}Co_y)_{50}Mn_{50-x}In_x$ arising from secondary heat-treatment and (ii) the effect of shell-ferromagnetism and the multiphase property on the magnetocaloric effect.

II. EXPERIMENT

We prepared samples of $Ni_{50-x}Co_xMn_{45}In_5$ with $x = 5$ and 8, a nearly full-Heusler $Ni_{44}Co_5Mn_{25}In_{26}$, and $Ni_{46}Co_5Mn_{35}In_{14}$ by arc-melting pure metals (99.99%) under argon atmosphere in a water-cooled Cu crucible. The samples with 5 at% In were used in shell-FM effect studies, and the 14 at%-In sample was used for studying the magnetocaloric effect. The full Heusler, which does not decompose according to Eq. (1) serves as a reference. The ingots were melted several times and were then sealed under 300-mbar argon in quartz tubes and annealed at 1073 K for five days followed by quenching in water at room temperature. The ingots were cut into slabs with a diamond wheel and further cut into thin, long specimens using a diamond wire saw. Some samples were further annealed at 750 K to examine shell-FM behavior and the effect of decomposition on the magnetocaloric effect. The compositions of the materials were determined with energy dispersive x-ray (EDX) spectroscopy using a scanning electron microscope (SEM).

We carried out x-ray diffraction (XRD) studies using a Panalytical X'pert Pro diffractometer with Cu-Kα radiation and analyzed the data using JANA2006 software [33]. Temperature-, field-, and time-dependent magnetizations, $M(T)$, $M(B)$, and $M(t)$, were measured using a superconducting quantum interference device (SQUID) magnetometer. The measurements were carried out in fields up to 5 T and in the temperature range $10 \leqslant T \leqslant 400$ K and further in the range $300 \leqslant T \leqslant 750$ K using an oven attachment.

III. RESULTS

We first present the structural properties and subsequently turn to the magnetic properties in view of shell-ferromagnetism and magnetocaloric effects.

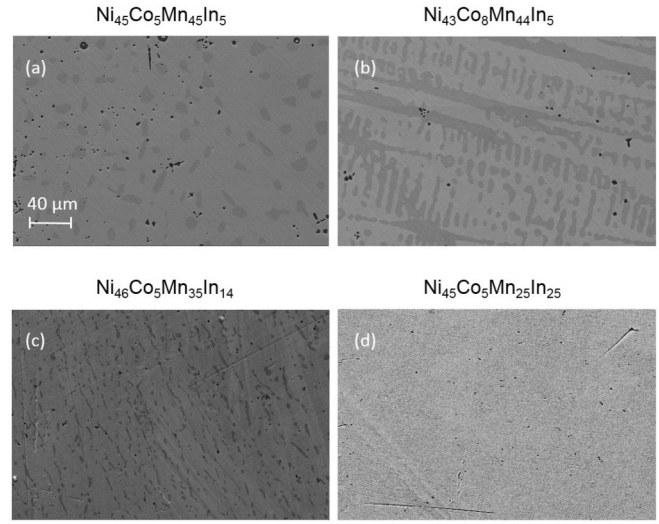

FIG. 1. SEM images of the samples with mean compositions (a) $Ni_{43}Co_8Mn_{44}In_5$, (b) $Ni_{45}Co_5Mn_{45}In_5$, (c) $Ni_{46}Co_5Mn_{35}In_{14}$, and (d) $Ni_{44}Co_5Mn_{25}In_{26}$. The provided scale in (a) is for all four images. See Table I for compositions of light and dark areas in (a)–(c).

A. Structural properties

1. SEM and EDX

The SEM images for the three off-stoichiometric Heusler samples given with their mean concentrations and the stoichiometric Heusler sample are shown in Fig. 1. Distinct light and dark gray regions in Figs. 1(a) to 1(c) indicate that the samples are inhomogeneous after annealing at 1073 K. The only sample that is homogeneous is $Ni_{44}Co_5Mn_{25}In_{26}$ as seen in Fig. 1(d). The dark regions make up about 20%, 10%, and 5% of the total coverage in Figs. 1(a), 1(b) and 1(c), respectively.

The results of the EDX measurements giving the mean concentration and the concentrations of the light and dark regions are collected in Tab. I. $Ni_{50-x}Co_xMn_{45}In_5$ with $x = 5$ and 8 mean concentrations decompose and form the light gray areas accommodating no more than about 5 at% Co, whereas the dark areas contain more Co and practically no In. The compound with mean composition $Ni_{46}Co_5Mn_{35}In_{14}$, often used in studying magnetocaloric effects, is also seen here to

TABLE I. Mean compositions and compositions of light and dark areas of the samples in at%.

Regions	Ni	Co	Mn	In
Mean	**45**	**5**	**45**	**5**
Light	44	5	46	5
Dark	44	10	46	0
Mean	**43**	**8**	**44**	**5**
Light	44	5	43	8
Dark	43	13	44	0
Mean	**46**	**5**	**35**	**14**
Light	46	4	35	15
Dark	47	18	35	0

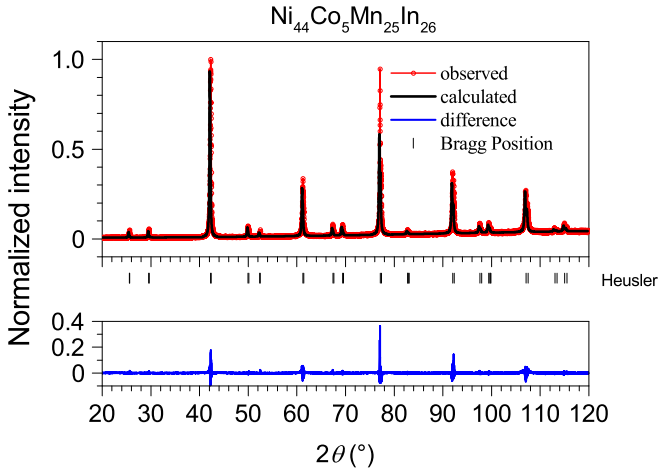

FIG. 2. XRD pattern for the full Heusler $Ni_{44}Co_5Mn_{25}In_{26}$.

have a mixed phase. These results are in good agreement with those of earlier studies [30].

2. XRD

We carried out XRD studies on both initial and 750-annealed states of samples used in studying the shell-FM effect and the MCE. We have also measured the spectrum for the full-Heusler $Ni_{44}Co_5Mn_{25}In_{26}$ as a reference. We have analyzed the spectrum of this sample shown in fig. 2 using the $Fm\bar{3}m$ space group. The spectrum shows typical features of the ordered Heusler $L2_1$ structure. We estimate the lattice parameter a to be 6.065 Å.

We show in fig. 3 the XRD patterns for the sample with mean composition $Ni_{45}Co_5Mn_{45}In_5$. The spectrum in fig. 3(a) corresponds to the initial state of the sample and is composed of tetragonal ($I/4mmm$) and cubic ($Fm-3m$) components, which are the light and dark regions, respectively, in the SEM images fig. 1. According to Tab. I, the light regions correspond to $L1_0$ $Ni_{44}Co_5Mn_{46}In_5$ with lattice parameters $a = 3.80$ Åand $c = 3.50$ Å. For the $Ni_{44}Co_{10}Mn_{46}$ cubic phase, $a = 3.69$ Å. We also detect a small amount of MnO in this sample.

When the sample is annealed at 750 K for 16 h, additional peaks appear at positions pertaining to the $L2_1$-Heusler structure. The most distinct ones correspond to (400) and (422) reflections. The refinement yields $a = 6.06$ Åfor the $L2_1$ phase. Due to the small size, and therefore, the weak intensity of these peaks, the uncertainty in a is larger than that determined for the full Heusler (fig. 2). Nevertheless, it lies within a limit where it can be identified as a lattice parameter pertaining to the Heusler phase. The tetragonal phase now has lattice parameters $a = 3.74$ Åand $c = 3.53$ Åindicating that this phase has become more Mn-rich corresponding more to those of $Ni_{50}Mn_{50}$. This result is in line with the reaction formula given in eq. 1. For the cubic phase, $a = 3.66$ Å.

The XRD spectra for the sample with the mean concentration $Ni_{43}Co_8Mn_{44}In_5$ shown in figs. 4(a) and 4(b) are similar to those shown in fig. 3 with the same structures appearing. The lattice constants of the light-region tetragonal $Ni_{44}Co_5Mn_{43}In_8$ phase are $a = 3.84$ Åand $c = 3.50$ Åcorresponding to a somewhat larger a-parameter than for the

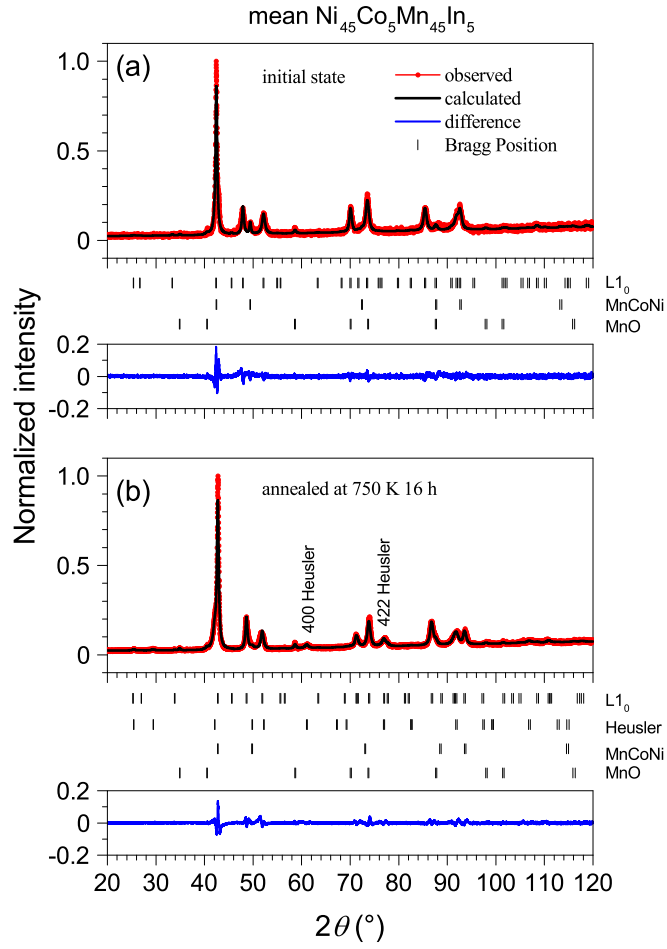

FIG. 3. XRD pattern for mean-$Ni_{45}Co_5Mn_{45}In_5$ in (a) the initial state and (b) the state obtained after annealing at 750 K for 16 h.

mean-$Ni_{45}Co_5Mn_{45}In_5$ sample (fig. 3). For the cubic phase, again $a = 3.66$ Å.

When this sample is annealed at 750 K for 16 h, decomposition within the light zones occurs leading to the spectrum seen in fig. 4(b) with distinctly emerging (400) and (422) Heusler-peaks. The analysis yields $a = 6.05$ Åalso for this case. The cell parameters for the tetragonal phase are now $a = 3.72$ Åand $c = 3.54$ Åshowing a similar change between initial and annealed states as with the sample discussed above in relation to fig. 3(b). Both analyses support the validity of the decomposition process occurring within the light regions according to eq. 1.

We now turn to the case of the sample with composition mean-$Ni_{45}Co_5Mn_{36}In_{14}$ in fig. 5, which we use to investigate the effect of secondary heat treatment on the MCE. As for the XRD presented for the samples introduced above, the initial state of this sample is also a mixture of tetragonal and cubic phases having compositions given in Tab. I. The lattice constants of the $L1_0$ phase are now $a = 3.94$ Åand $c = 3.47$ Åwith a being considerably larger than for the initial states of the samples discussed in conjunction with figs. 3 and 4. For the cubic phase $a = 3.66$ Å, which does not vary appreciably from those of the other two samples.

The XRD spectrum for the 750 K-annealed case is shown in fig. 5(b). Unlike for the previous two samples the spectrum

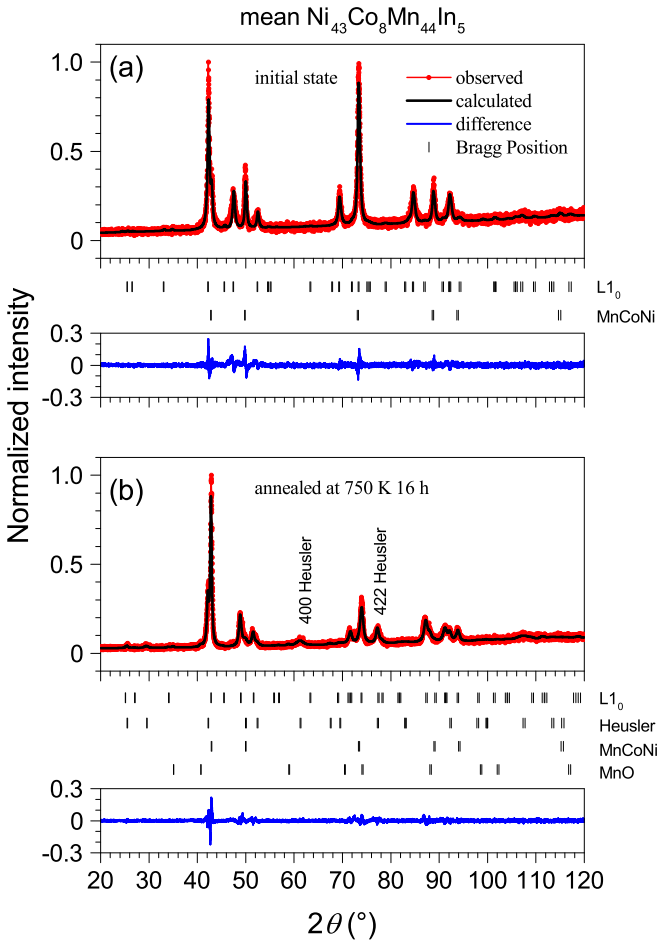

FIG. 4. XRD pattern for mean-$Ni_{43}Co_8Mn_{44}In_5$ in (a) the initial state and (b) the state obtained after annealing at 750 K for 16 h.

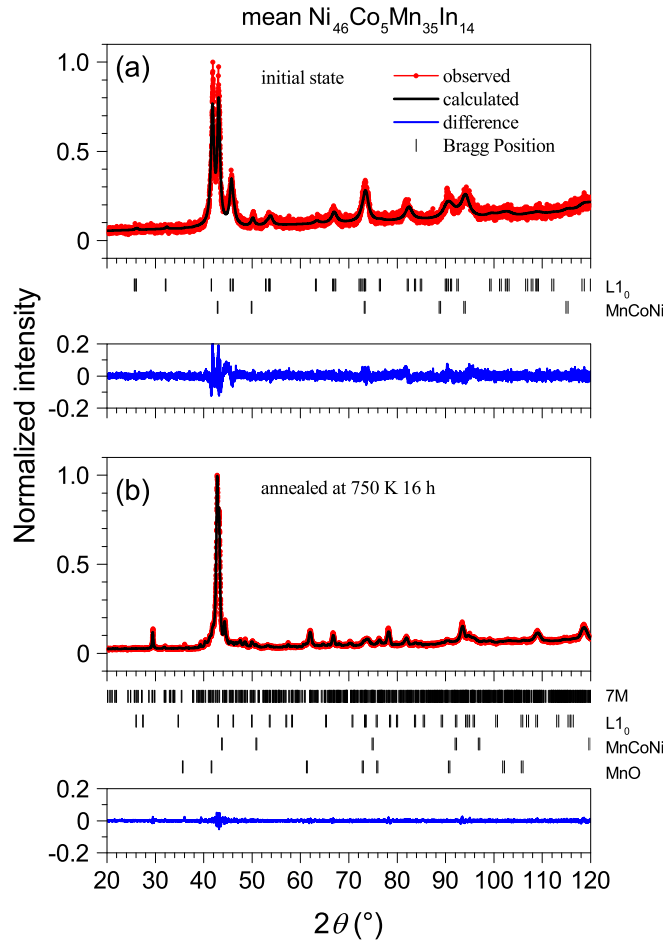

FIG. 5. XRD pattern for mean-$Ni_{45}Co_5Mn_{36}In_{14}$ in (a) the initial state and (b) the state obtained after annealing at 750 K for 16 h.

is now described by a mixture of $L1_0$, an incommensurately modulated 7M, and a cubic phase. The 7M structure is monoclinic described by the superspace group P2/m(a0g)00. The cell parameters are $a = 4.30$ Å, $b = 5.44$ Å, $c = 4.40$ Å $\alpha = 90^\circ$ Å $\beta = 91.3^\circ$, $\gamma = 90^\circ$, and the modulation vector is $q = 0.34$. The cubic phase has $a = 3.65$ Å, which is nearly the same as those for the other cases presented above.

B. Magnetic properties

With the structural analysis presented above, we now turn to the shell-FM properties and the effect of decomposition on the magnetocaloric properties. In the presence of 5 at.% Co, we expect the decomposition to occur according to the reaction

$$(25/x)(Ni_{0.9}Co_{0.1})_{50}Mn_{50-x}Z_x \rightarrow (Ni_{0.9}Co_{0.1})_{50}Mn_{25}Z_{25} + [(25/x) - 1]Ni_{50}Mn_{50} \quad 0 < x \leqslant 25. \quad (2)$$

where the first term on the right is the shell-FM precipitate.

1. *Magnetic properties of near-stoichiometric* $Ni_{44}Co_5Mn_{25}In_{26}$

We can sort out the magnetic properties of the precipitates by first identifying their Curie temperature T_C. Therefore, it is first necessary to know T_C of $Ni_{45}Co_5Mn_{25}In_{25}$. Figure 6 shows $M(T)$ for the near-stoichiometric $Ni_{44}Co_5Mn_{25}In_{26}$ compound. We carried out a sequence of temperature-cycling $M(T)$ measurements in 1 T as seen in Fig. 6(a). Cycling $M(T)$ between 300 and 500 K is reversible. However, taking the sample from its initial state at 300 K (open-red) to a final annealed state at 750 K (black) causes T_C to increase due to the increase of $L2_1$ ordering [26]. We show $M(T)$ in 5 mT before and after annealing in Fig. 6(b). This low-field measurement allows T_C to be determined as 354 and 373 K for the initial and final states, respectively. The inset shows $M(B)$ at 10 K for the annealed state, for which the saturation magnetization is about 115 Am^2kg^{-1}.

2. *Shell-FM properties*

To examine the properties of the shell-FM effect in Co-incorporating Ni-Mn-In compounds, we studied the decomposition process by measuring $M(t)$, and $M(T)$, the later obtained by a sequential annealing protocol. We also measured $M(B)$ in both initial and decomposed states to gain more detailed information on the magnetic properties. We carry out the studies for the two compositions mean-$Ni_{45}Co_5Mn_{45}In_5$ and mean-$Ni_{43}Co_8Mn_{44}In_5$. In the initial state these samples are AF, which we verify by the linear behavior of $M(B)$ at 10

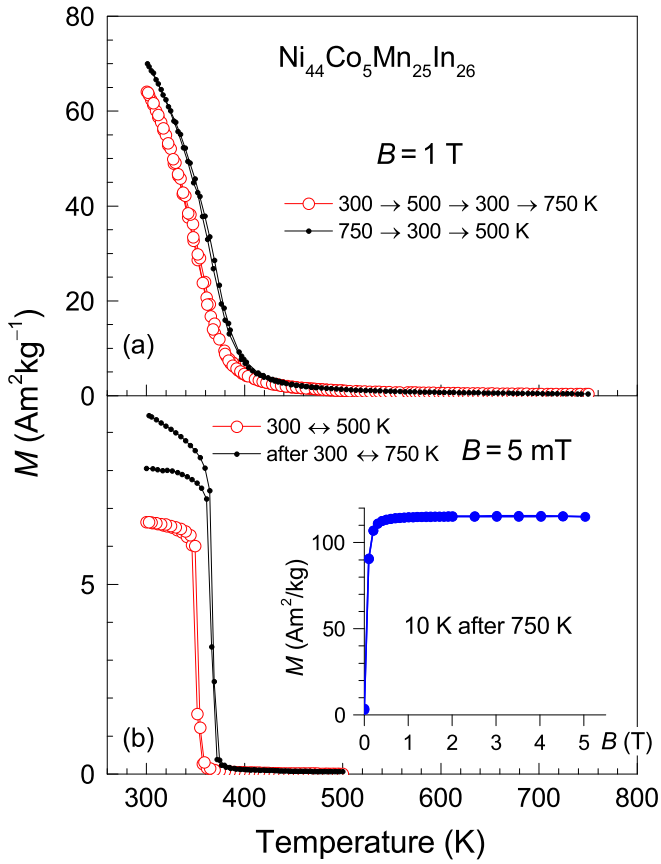

FIG. 6. $M(T)$ for the near-stoichiometric $Ni_{44}Co_5Mn_{25}In_{26}$ compound. (a) A sequence of temperature-cycling measurements made in 1 T taking the sample from its initial state (open-red) to a final annealed state (black) showing the increase in T_C due to increase of $L2_1$ ordering. (b) $M(T)$ in 5 mT before and after annealing. The inset shows $M(B)$ at 10 K for the annealed state. The saturation magnetization is about 115 Am^2kg^{-1}.

and 300 K as seen in Fig. 7. This is an expected result for such low In concentrations. There is no evidence of any FM background in these data arising from segregated Ni-Co-Mn (Fig. 1). However, this becomes evident in the $M(T)$-data which we present next.

Sequential annealing experiments are carried out by raising the temperature to a certain value, returning back to room temperature, and raising the temperature again to a higher value than the previous maximum temperature; and so on. We give the results of such experiments for both samples in Fig. 8. The details of the protocol are given in the legends of Figs. 8(a) and 8(b). The data are obtained in 5 T. Between 300 and 500 K the data are reversible for both samples. In this range, $M(T)$ increases steadily with increasing temperature as seen in the detailed plots in Figs. 8(c) and 8(d). Such behavior is typical for an antiferromagnet and is consistent with the behavior of $M(B)$ shown in Fig. 8. However, $M(T)$ initially has a high background caused by the presence of FM Ni-Co-Mn impurities (Table I). When the temperature is raised to 700 K, $M(T)$ does not return to its original value at 300 K for both samples. This behavior becomes even more distinct when the temperature is increased to 750 K and reduced back

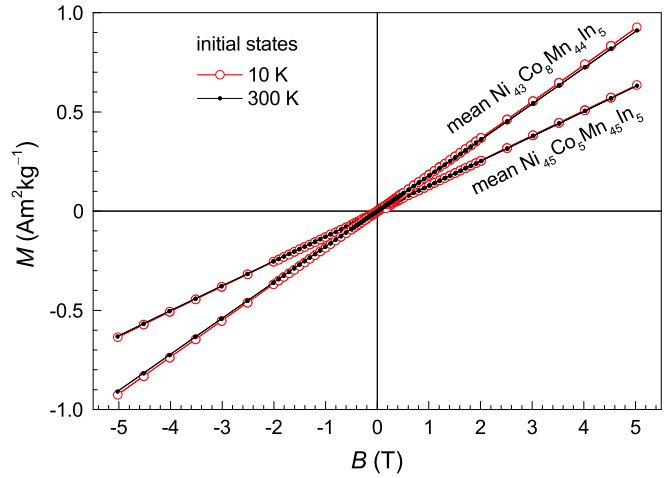

FIG. 7. $M(B)$ for mean-$Ni_{45}Co_5Mn_{45}In_5$ and mean-$Ni_{43}Co_8Mn_{44}In_5$ showing the linear behavior at 10 and 300 K.

to 300 K. At these measurement steps, Heusler precipitates begin to form and FM interactions set in so that the data indicate a Curie temperature T_C close to 350 K. As will be seen below, T_C is better determined from $M(T)$ of samples that decompose over a longer period of time. We also find that when running sequence 5 in Fig. 8(a), the sample undergoes a reverse martensitic transition to the cubic austenite state, at least partially, beginning at about 730 K. It returns back to the martensite state on recooling. Mean-$Ni_{43}Co_8Mn_{44}In_5$ has a lower martensitic transition temperature, so that the complete transformation can be observed. These are further discussed in Sec. IV B.

To provide further support for the occurrence of decomposition, we mounted new samples in their initial states and

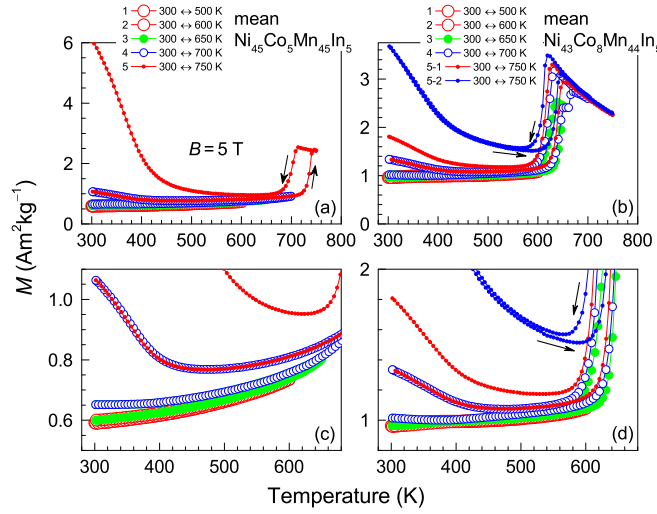

FIG. 8. High-temperature sequential annealing for (a) mean-$Ni_{45}Co_5Mn_{45}In_5$ and (b) mean-$Ni_{43}Co_8Mn_{44}In_5$. Sequential annealing is performed under 5 T according to the protocols given in the legends of (a) and (b). Steps 1 and 2 are shown with the same symbol since very little change occurs on cycling between 300 and 600 K for both samples. (c) and (d) show expanded plots of parts (a) and (b), respectively, giving details of the deviations from step 1.

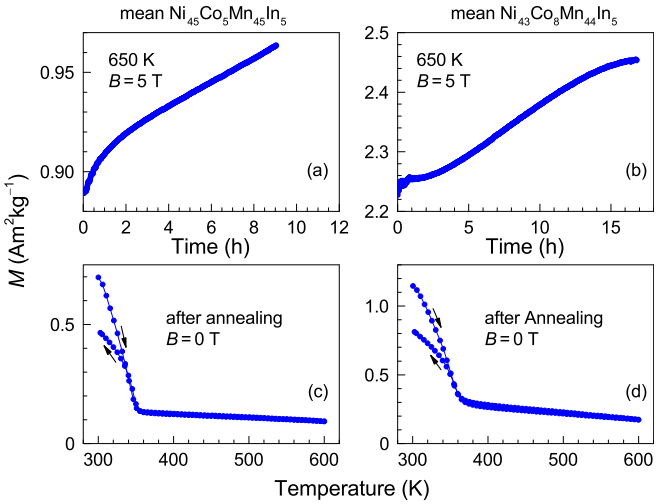

FIG. 9. (a) $M(t)$ for (a) mean-$Ni_{45}Co_5Mn_{45}In_5$ and (b) mean-$Ni_{43}Co_8Mn_{44}In_5$ obtained at $T_a = 650$ K and 5 T. (c) and (d) $M(T)$ in remanence after recording $M(t)$ in parts (a) and (b), respectively.

carried out $M(t)$ measurements at 650 K. We then measured $M(T)$ in remanence. The results are given in Fig. 9. $M(T)$ increases with time when the samples are held at 650 K under 5 T as seen in Figs. 9(a) and 9(b). The increase is caused by the emerging FM Heusler precipitates that become embedded in a co-emerging NiMn surrounding, by which the Heusler/NiMn interface spins become pinned.

After the temperature is reduced and the field is removed, we measured $M(T)$ in remanence. The results are shown in Figs. 9(c) and 9(d). Here, the position of T_C is determined to be around 345 and 360 K, which are close to the value obtained for the near-stoichiometric compound, for which $M(T)$ is shown in Fig. 6. $M(T)$ drops as the temperature reaches T_C, above which $M(T)$ decreases steadily up to 600 K. The decrease is caused by the progressive weakening of the pinning as the temperature increases. On returning to 300 K, $M(T)$ does not reach its original value but remains somewhat lower. This is caused by further segregation occurring at 600 K, however, this time in the absence of a magnetic field since $M(T)$ is measured in remanence. Therefore, the spins of shells of the newly emerging or further growing precipitates point randomly and contribute to a reduction in the total magnetization causing $M(T)$ to be smaller at 300 K.

Directly after the sequential annealing measurements shown in Fig. 8, we measured $M(B)$ of these samples at 300 and 500 K. At 300 K, the system is expected to be partially in a FM state according to step 5 in Figs. 8(a) and 8(b). As we show in Figs. 10(a) and 10(b), the 300 K-data reflect indeed a FM response arising from the segregated FM Heusler components. The data at 500 K appear to show dominant AF behavior. However, when viewed more closely in the insets, the data show a 20 mT-wide hysteresis shifted vertically. The shift is more pronounce for the Co_5-sample as seen in Fig. 10(b). The vertical shift is an indication that the loop between +5 and −5 T is a minor loop. This is a typical property of the shell-FM effect, where the shell spins become pinned in the annealing-field direction by the AF matrix so fields in the order of 20 T are required to rotate them [24].

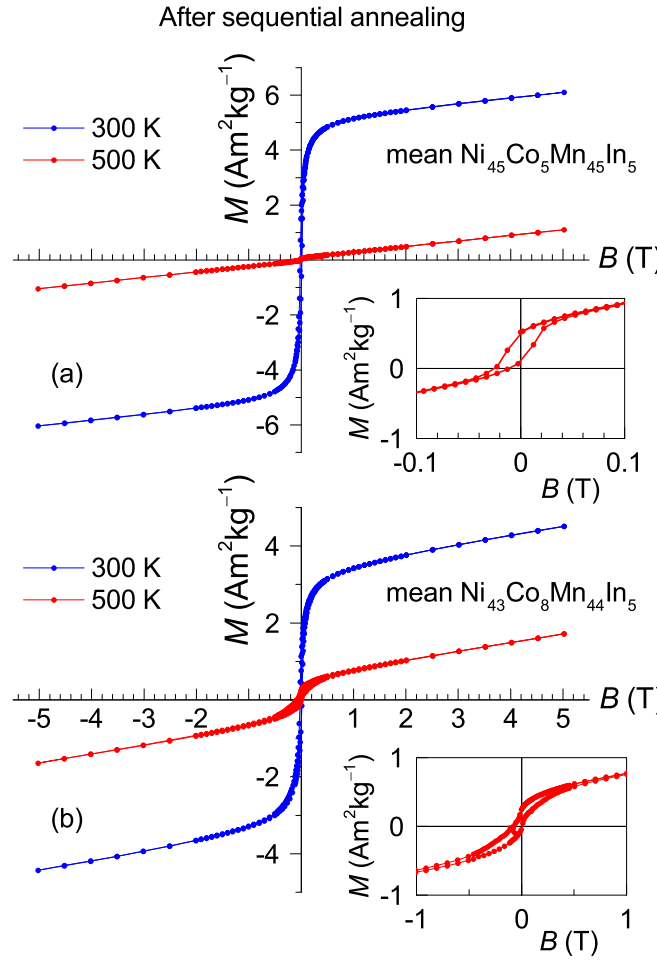

FIG. 10. $M(B)$ after sequential annealing (Fig. 8) for (a) mean-$Ni_{45}Co_5Mn_{45}In_5$ and (b) mean-$Ni_{43}Co_8Mn_{44}In_5$ at 300 K (blue) and 500 K (red). Insets show the 500 K-data focusing on the vertical shift and the hysteresis in the low-field area.

3. Magnetocaloric effects

As in Co-free off-stoichiometric Heusler alloys, the Co-incorporating alloys also decompose and exhibit the shell-FM effect. The Co-incorporating alloys are widely studied for their magnetocaloric properties and are known to exhibit large entropy-changes around room temperature. This makes them attractive for their possible use in room-temperature magnetic cooling devices. However, the decomposition can have consequences on the magnetocaloric properties and requires a closer look.

$Ni_{46}Co_5Mn_{35}In_{14}$ shows particularly large magnetocaloric effects around room temperature and has been widely studied. This compound is generally claimed to be homogeneous. However, the images in Fig. 1(c) and the compositions in Table I show that inhomogeneities are also present in this system. Therefore, we study the magnetization and the magnetocaloric properties of this compound in its initial state and in a state where the sample is subjected to secondary heat treatment at 750 K for 16 h. The results are shown in Fig. 11 for $M(T)$ measured in 5 mT under ZFC and FC conditions for both initial and annealed states. T_C increases from 358 to 368 K when the sample is annealed. The martensite-start

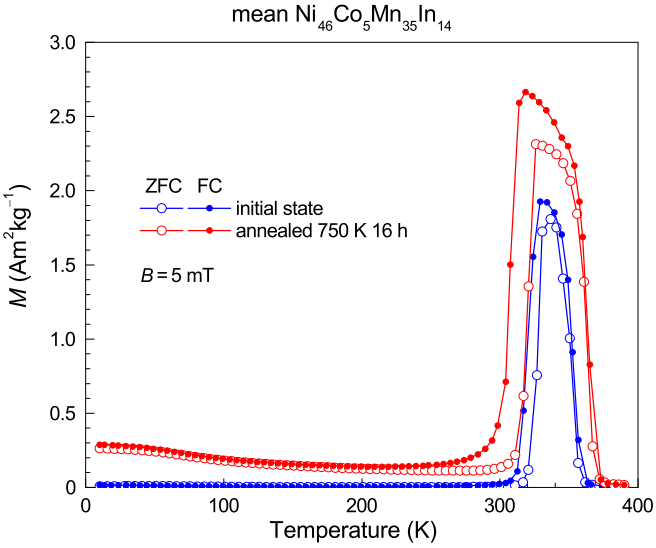

FIG. 11. (a) $M(T)$ measured in 5 mT for mean-$Ni_{46}Co_5Mn_{35}In_{14}$ in a ZFC (open symbols)-FC (closed symbols) sequence of measurements in initial and annealed states.

temperature M_s, determined as the peak-temperature of the FC-curve, shows the opposite effect and decreases from 328 to 319 K. The hysteresis width also increases from 6.5 to 13.5 K on annealing.

To estimate the magnetocaloric effect for both states, we measured $M(B)$ around the transition temperature for each case. We show the results in Fig. 12. Prior to the measurements the sample-temperatures were brought down to 200 K, well within the martensite state, and subsequently to the measuring temperature. At temperatures around the transition region $M(B)$ shows features related to the presence of field-induced transformations from martensite to austenite.

For both cases, we calculated ΔS using the relationship

$$\Delta S(T, \Delta B) = \int_{B_1}^{B_2} \left(\frac{\partial M(T, B)}{\partial T} \right)_B dB, \tag{3}$$

and numerically integrating it using

$$| \Delta S(T, \Delta B) | = \sum_i \frac{M_i - M_{i+1}}{T_{i+1} - T_i} \Delta B. \tag{4}$$

Here M_i and M_{i+1} are magnetization values measured at temperature T_i and T_{i+1}, respectively.

ΔS versus T for both states of the sample is plotted in Fig. 13. ΔB is the field-change referenced to zero-field. The peak values in ΔS are at 23 $Jkg^{-1}K^{-1}$ and 28 $Jkg^{-1}K^{-1}$ for the initial and annealed states, respectively.

IV. DISCUSSION

A. Structure

Compositions around $Ni_{45}Co_5Mn_{36}In_{14}$ are often studied for their magnetocaloric properties. It appears that these compounds with compositions around 5 at% Co are unstable with respect to the formation of a multiphase compound incorporating In-poor fcc inclusions and a main off-stoichiometric Heusler matrix. This occurs in samples slowly cooled from

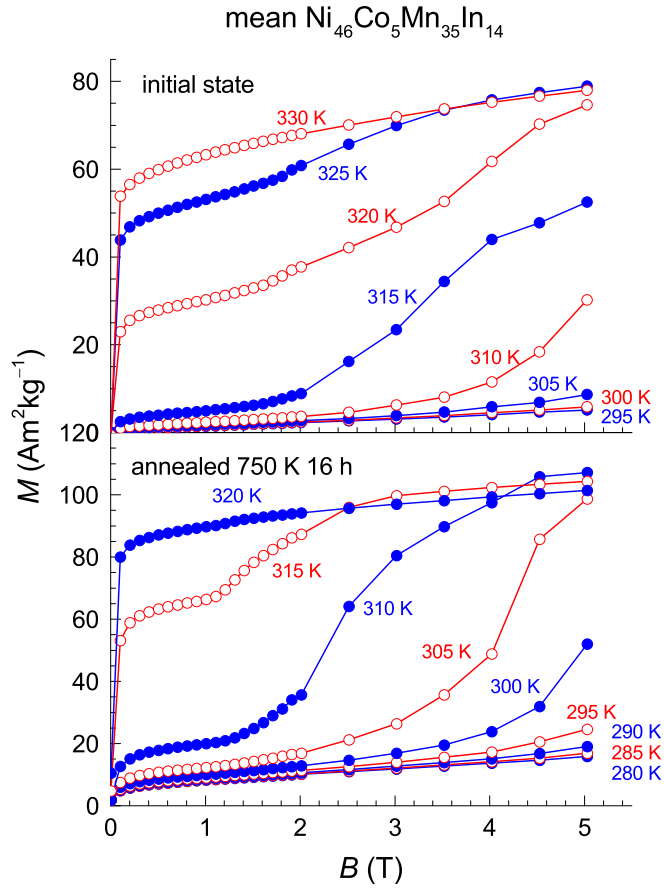

FIG. 12. $M(B)$ for (a) the initial and (b) the 750 K-annealed states of mean-$Ni_{46}Co_5Mn_{35}In_{14}$ at temperatures around the martensitic transition.

initial heat-treatment temperatures around 900° C [30] as well as those that are quenched from these temperatures; as in the present study. When these samples are subjected to secondary heat-treatments around 600 to 750 K, a further decomposition effect occurs; namely, the shell-FM effect. In this case the light areas in Fig. 1 undergo a decomposition according to Eq. (2) within themselves. This is verified by the XRD and magnetization studies. The presence of multiple phases in quaternary Heuslers is not limited to these alloys but are also encountered in various other systems [31,34,35].

The full Heusler compound $Ni_{45}Co_5Mn_{25}In_{25}$ is single-phase and does not decompose on secondary heat-treatment (Fig. 1) since it is the composition corresponding to the boundary of the miscibility gap determined by the reaction in Eq. (2). However, the secondary heat-treatment at 750 K causes T_C to increase (Fig. 6). This increase is expected to be caused by the increase in the degree of order of the $L2_1$-phase [26,36].

All in all, there are three nonequilibrium events in Ni-Mn-In-based Heusler compounds that incorporate Co: (1) Segregation due to the initial heat-treatment into a main Heusler phase and and an In-free phase; (2) the occurrence of shell-FM decomposition on secondary heat-treatment; and (3) the increase in $L2_1$ ordering of the Heusler phase leading to an increase in T_C.

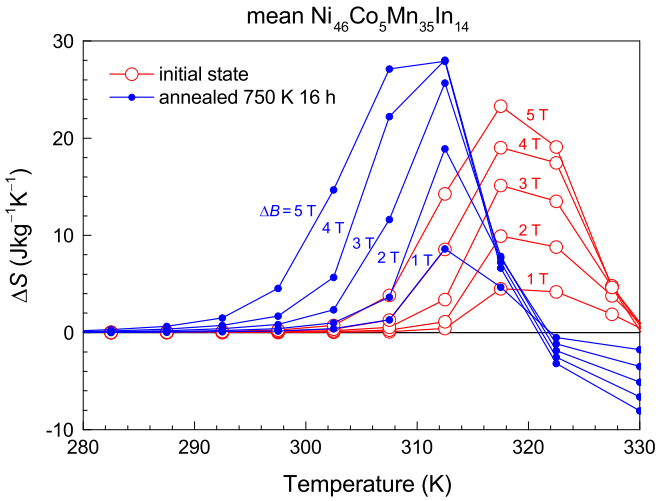

FIG. 13. The temperature dependence of the inverse magnetocaloric effect plotted as ΔS vs. T for the initial and the 750 K-annealed states of mean-$Ni_{46}Co_5Mn_{35}In_{14}$. ΔB shows the field-change from zero-field.

The XRD data showing the emerging Heusler peaks are in line with a previous study on shell-ferromagnetism, where the development of the Heusler precipitates are examined as a function of annealing-time, and annealing-temperature T_a [37]. In this study the size of the precipitates was determined by Scherrer analysis. For a secondary heat treatment at 750 K for 16 h, the size of the precipitates in our case is expected to be around 20–30 nm.

B. Shell-FM properties

The shell-FM properties were studied for two compositions with low In-content. They show two interesting effects which are the change in the martensite transition temperature T_m as annealing progresses and the migration of Co into the precipitate as well as into the matrix. We discuss these below.

The phases relevant for the shell-FM effect are those with the light contrast in Fig. 1, namely $Ni_{44}Co_5Mn_{46}In_5$ and $Ni_{44}Co_5Mn_{43}In_8$. The sample with 8 at% In has a lower valence electron concentration, e/a, so that T_m lies lower. However, we see in Fig. 8(b) that the T_m shifts to lower values as the annealing progresses. This is opposite to the effect observed for the shell-FM effect in $Ni_{50}Mn_{45}Sb_5$, where T_m increases as the annealing progresses [38]. This case is more comprehensible since, as the annealing progresses, the $L1_0$-phase surrounding the precipitate becomes more Mn-rich and Sb-poor so that e/a would increase and cause the martensitic transition temperature to increase as well. The same should be true for $Ni_{44}Co_5Mn_{43}In_8$. However, to account for the decrease, it would be necessary to require a counteracting effect. It is known that adding Co in place of Ni in Ni-Mn-based Heuslers leads to a decrease in T_m and an increase in T_C. The precipitate can only accommodate a Co content of less than 5 at%. Therefore, the remaining Co has to go into the $L1_0$ matrix and overcompensate the increase in T_m caused by the increase in the Mn-concentration.

Together with the shift of T_m, it is necessary to understand where Co actually migrates. $M(T)$ measurements in remanence yield a T_C of about 350–360 K for the precipitates as seen in Figs. 9(c) and 9(d). This corresponds to T_C for the full Heusler $Ni_{50}Co_5Mn_{25}In_{25}$. In $Ni_{50}Mn_{25}In_{25}$, the precipitates formed as a result of decomposition have $T_C = 300$ K. Therefore, in the present case, the precipitate is enriched with Co. This has the advantage that the precipitate has a saturation magnetization M_s of 115 Am^2kg^{-1} which is larger than that of $Ni_{50}Mn_{25}In_{25}$ precipitates with $M_s = 70$ Am^2kg^{-1}.

C. Magnetocaloric effect

Ni-Co-Mn-In compounds have been widely studied particularly for their favorable magnetocaloric properties even though the composition-range for substituting Ni with Co is very limited. In many cases, the compound is not single phase which impedes favorable magnetocaloric properties, and it would be useful to prepare such materials with a single-phase. Our results show that as in ternary Ni-Mn-based Heuslers, a miscibility gap between the full Heusler and NiMn exists also in the quaternary Co-incorporating systems. Next to effects related to compositional inhomogeneities due to excess Co, the decomposition of the off-stoichiometric Heusler phase also has effects on the magnetocaloric properties of these materials. A secondary heat treatment immediately reveals a change in the magnetocaloric properties (Fig. 13) which could be favorable or unfavorable depending on how it will be employed. The secondary heat treatment at these compositions result in a decomposition rather than solely a change in the magnetic ordering temperature.

V. CONCLUSION

Ni-Co-Mn-In can accommodate only up to about 5 at% Co, and a Co-concentration more than this gives rise to a multiphase systems. We studied shell-FM decomposition in Ni-Co-Mn-In systems and studied its implications on the magnetocaloric properties of these materials. For the shell-FM effect, we enhance the FM exchange of the precipitates by introducing Co into the precipitates and thereby increasing their T_C and M_s. This improves their energy product. For the magnetocaloric effect, we find that the secondary heat treatment gives rise to large changes in the entropy-change properties. Therefore, shell-FM precipitation is linked to the magnetocaloric properties and care must be taken in preparing the metallurgical state of the material for a chosen application.

ACKNOWLEDGMENTS

This work was supported by Deutsche Forschungsgemeinschaft (Project No. 405553726-CRC/TRR 270). The authors acknowledge support from the Turkish Scientific and Technological Research Council (Project No. 1059B191701241), the Deutsche Akademisches Austausch Dienst, and the Government of the Russian Federation (Grant No. 075-15-2019-1886).

[1] P. J. Webster, K. R. A. Ziebeck, S. L. Town, and M. S. Peak, Philos. Mag. B **49**, 295 (1984).

[2] K. Ullakko, J. K. Huang, C. Kantner, R. C. OHandley, V. V. Kokorin, Appl. Phys. Lett. **69**, 1966 (1996).

[3] A. Sozinov, A. A. Likhachev, N. Lanska, and K. Ullakko, Appl. Phys. Lett. **80**, 1746 (2002).

[4] A. Planes, L. Mañosa, and M. Acet, J. Phys.: Condens. Matter **21**, 233201 (2009).

[5] M. Acet, L. Mañosa, and A. Planes, in Handbook of Magnetic Materials Vol. 19, edited by K. H. J. Buschow, (Elsevier, Amsterdam, 2011), pp. 231–289.

[6] R. Kainuma, Y. Imano, W. Ito, Y. Sutou, H. Morito, S. Okamoto, O. Kitakami, K. Oikawa, A. Fujita, T. Kanomata, and K. Ishida, Nature **439**, 957 (2006).

[7] T. Krenke, E. Duman, M. Acet, E. F. Wassermann, X. Moya, L. Mañosa, A. Planes, E. Suard, and B. Ouladdiaf, Phys. Rev. B **75**, 104414 (2007).

[8] T. Krenke, E. Duman, M. Acet, E. F. Wassermann, X. Moya, L. Mañosa, and A. Planes, Nat. Mater. **4**, 450 (2005).

[9] K. Koyama, H. Okada, K. Watanabe, T. Kanomata, R. Kainuma, W. Ito, K. Oikawa, and K. Ishida, Appl. Phys. Lett. **89**, 182510 (2006).

[10] V. K. Sharma, M. K. Chattopadhyay, K. H. B. Shaeb, A. Chouhan, and S. B. Roy, Appl. Phys. Lett. **89**, 222509 (2006).

[11] M. Khan, I. Dubenko, S. Stadler, and N. Ali, Appl. Phys. Lett. **91**, 072510 (2007).

[12] Z. Li, C. Jing, J. Chen, S. Yuan, S. Cao, and J. Zhang, Appl. Phys. Lett. **91**, 112505 (2007).

[13] A. Cakir, M. Acet, and M. Farle, Sci. Rep. **6**, 28931 (2016).

[14] F. Casper, T. Graf, S. Chadov, B. Balke, and C. Felser, Semicond. Sci. Technol. **27**, 063001 (2012).

[15] I. Dubenko, M. Khan, A. K. Pathak, B. R. Gautam, S. Stadler, and N. Ali, J. Magn. Magn. Mater. **321**, 754 (2009).

[16] T. Kihara, X. Xu, W. Ito, R. Kainuma, and M. Tokunaga, Phys. Rev. B **90**, 214409 (2014).

[17] T. Gottschall, K. P. Skokov, F. Scheibel, M. Acet, M. G. Zavareh, Y. Skourski, J. Wosnitza, M. Farle, and O. Gutfleisch, Phys. Rev. Applied. **5**, 024013 (2016).

[18] P. J. Shamberger and F. S. Ohuchi, Phys. Rev. B **79**, 144407 (2009).

[19] I. Titov, M. Acet, M. Farle, D. González-Alonso, L. Mañosa, A. Planes, and T. Krenke, Appl. Phys. **112**, 073914 (2012).

[20] V. Basso, C. P. Sasso, K. P. Skokov, O. Gutfleisch, and V. V. Khovaylo, Phys. Rev. B **85**, 014430 (2012).

[21] V. Provenzano, E. D. Torre, L. H. Bennett, and H. El Bidweihy, Physica B **435**, 138 (2014).

[22] T. Gottschall, E. S. Taulats, L. Mañosa, A. Planes, K. P. Skokov, and O. Gutfleisch, Appl. Phys. Lett. **110**, 223904 (2017).

[23] A. Cakir, M. Acet, U. Wiedwald, T. Krenke, and M. Farle, Acta Mater. **127**, 117 (2017).

[24] F. Scheibel, D. Spoddig, R. Meckenstock, T. Gottschall, A. Cakir, T. Krenke, M. Farle, O. Gutfleisch, and M. Acet, Appl. Phys. Lett. **110**, 192406 (2017).

[25] J. A. Monroe, I. Karaman, B. Basaran, W. Ito, R. Y. Umetsu, R. Kainuma, K. Koyama, and Y. I. Chumlyakov, Acta Mater. **60**, 6883 (2012).

[26] Y. Wang, D. Salas, T. C. Duong, B. Medasani, A. Talapatra, Y. Ren, Y. I. Chumlyakov, I. Karaman, and R. Arróyave, J. Alloys Compd. **781**, 479 (2019).

[27] N. M. Bruno, S. Wang, I. Karaman, and Y. I. Chumlyakov, Sci. Rep. **7**, 40434 (2017).

[28] D. L. Schlagel, R. W. McCallum, and T. A. Lograsso, J. Alloys Compd. **463**, 38 (2008).

[29] W. M. Yuhasz, D. L. Schlagel, Q. Xing, K. W. Dennis, R. W. McCallum, and T. A. Lograsso, J. Appl. Phys. **105**, 07A921 (2009).

[30] K. Reclik, K. P. T. Goryczka, M. Kubiztal, and D. Stróż, Solid State Phenomena **203-204**, 240 (2013).

[31] P. Lazpita, M. Sasmaz, E. Cesari, J. M. Barandiaran, J. Gutierrez, and V. A. Chernenko, Acta Mater. **109**, 170 (2016).

[32] T. Krenke, Asli Cakir, F. Scheibel, M. Acet, and M. Farle, J. Appl. Phys. **120**, 243904 (2016).

[33] V. Petricek, M. Dusek, and L. Palatinus, Z. Kristallogr. **229**, 345 (2014).

[34] C. Tan, Z. Tai, K. Zhang, X. Tian, and W. Cai, Sci. Rep. **7**, 2e10 (2017).

[35] P. Lazpita, M. Sasmaz, J. M. Barandiaran, and V. A. Chernenko, Acta Mater. **155**, 95 (2018).

[36] N. M. Bruno, D. Salas, S. Wang, I. V. Roshchin, R. Santamarta, R. Arroyave, T. Duong, Y. I. Chumlyakov, and I. Karaman, Acta Mater. **142**, 95 (2018).

[37] L. Dincklage, F. Scheibel, A. çakır, M. Farle, and M. Acet, AIP Adv. **8**, 025012 (2018).

[38] Z. Wanjiku, A. Cakir, F. Scheibel, M. Farle, and M. Acet, J. Appl. Phys. **125**, 043902 (2019).